Selectivity and Cooperativity of Modulatory Ions in a Neurotransmitter Receptor

Ranjit Vijayan,[†‡] Andrew J. R. Plested,[§] Mark L. Mayer,[§] and Philip C. Biggin[†*]
[†]Department of Biochemistry, [‡]Life Sciences Interface Doctoral Training Centre, University of Oxford, Parks Road, Oxford, United Kingdom; and [§]Laboratory of Cellular and Molecular Neurophysiology, Porter Neuroscience Research Center, National Institute of Child Health and Human Development, National Institutes of Health, Department of Health and Human Services, Bethesda, Maryland

ABSTRACT Ions play a modulatory role in many proteins. Kainate receptors, members of the ionotropic glutamate receptor family, require both monovalent anions and cations in the extracellular milieu for normal channel activity. Molecular dynamics simulations and extensive relative binding free energy calculations using thermodynamic integration were performed to elucidate the rank order of binding of monovalent cations, using x-ray crystal structures of the GluR5 kainate receptor dimers with bound cations from the alkali metal family. The simulations show good agreement with experiments and reveal that the underlying backbone structure of the binding site is one of the most rigid regions of the protein. A simplified model where the partial charge of coordinating oxygens was varied suggests that selectivity arises from the presence of two carboxylate groups. Furthermore, using a potential of mean force derived from umbrella sampling, we show that the presence of cations lower the energy barrier for anion approach and binding in the buried anion binding cavity.

INTRODUCTION

Ionotropic glutamate receptors (iGluRs) encompass a large family of tetrameric ligand-gated cation channels that are activated by the endogenous ligand glutamate (1,2). They are responsible for a significant proportion of excitatory neurotransmission in the central nervous system. Hence, inevitably, abnormal functioning of these receptors is associated with many neurodegenerative diseases including Alzheimer's, Huntington's, and Parkinson's disease. Broadly, based on gene sequences and ligand selectivity, the iGluR family consists of three major subtypes: α-amino-3-hydroxy-5-methyl-4-isoxazolepropionic acid (AMPA); kainate; and *N*-methyl-*D*-aspartate (NMDA) receptors (1–3). NMDA receptors require both glycine and glutamate for activation (4), whereas AMPA and kainate receptors are activated by glutamate alone, and thus have been regarded as functionally similar (5). Kainate receptors were identified by their ability to selectively bind the agonist kainate (originally isolated from a marine alga (6)) with nanomolar affinity. The kainate receptor family consists of subunits GluR5–7 and KA1–2 (1). Kainate receptors have both presynaptic and postsynaptic functional roles with a range of kinetic responses (7,8).

Ion binding to proteins is a common phenomenon required for preventing aggregation, maintaining electroneutrality, and allowing close packing. But in addition, ions can regulate the activity of biological macromolecules via allosteric mechanisms. Ions exist as hydrated entities in bulk solution (9). To bind favorably, a protein must compensate for the energetic penalty involved in partly or fully removing the hydration shell of an ion. Ions of differing sizes and valences, like sodium, chloride, calcium, magnesium, and zinc, are present in biological tissues, bind to, and modulate a range of receptors (10–13). Unusually, kainate subtype glutamate receptors have been shown to require both anions and cations in the extracellular milieu for receptor activation and these ions regulate the rate of onset of desensitization (14–16). We recently reported crystal structures of the cation binding sites in kainate receptors (see Fig. 1). There are two sodium-binding sites, each 8 Å from a binding site for anions, but the extent of interaction between the ion binding sites and underlying mechanism of selectivity for sodium are currently unknown.

Computational methods have been used to study aspects of iGluR dynamics and ligand binding (17–22). More generally, they allow one to compute the free energy change associated with many biological processes (23). Absolute and relative binding free energies have been derived for many biological systems using alchemical transformations that are physically impossible but computationally accessible, e.g., the binding free energy of ligands and water molecules in cavities and bindings sites (24–26). Such calculations can be exploited to allow us to predict the affinity of different ions in binding sites in proteins. Potentials of mean force (PMF), i.e., the change in free energy as a function of a defined reaction coordinate, derived from umbrella sampling (27), adaptive biasing simulations (28), or steered molecular dynamics (MD) (29,30) have been used to describe free energy barriers associated with many processes including translocation of ions (31,32) and other molecules (30) through channels, opening/closing of an AMPA receptor GluR2 ligand binding domain (20), and finding the preferred location of small molecules and lipids in model lipid bilayers (33).

Submitted August 18, 2008, and accepted for publication November 13, 2008.

*Correspondence: philip.biggin@bioch.ox.ac.uk

Editor: Peter Tieleman.

0006-3495/09/03/1751/10 $2.00
doi: 10.1016/j.bpj.2008.11.039

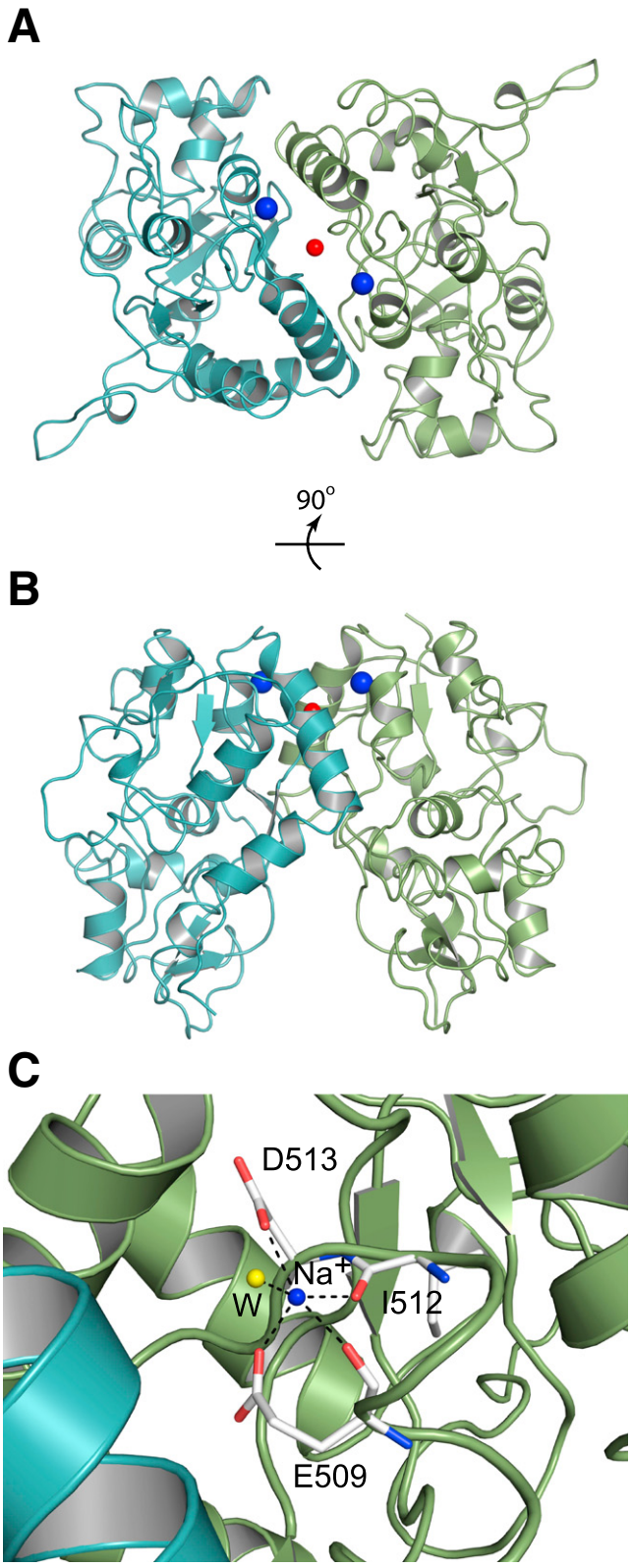

FIGURE 1 (*A*) Top view and (*B*) side view of a cartoon representation of GluR5 (3C32) dimer with subunits in green and blue. Na^+ and Cl^- ions are displayed as blue and red spheres, respectively (not to scale). (*C*) Closeup of one of the sodium binding sites. The oxygen of a water molecule coordinating the sodium is shown as a yellow sphere (not to scale).

In this article, we report on the calculation of the relative binding free energy of ions from the alkali metal family, with respect to crystal structures of GluR5 bound to the partial agonist kainic acid (which we recently solved in complex with a series of allosteric cations (34)). We address the underlying principle of selectivity by using a subset of protein atoms, ions and water molecules where we vary the strength of binding-site electrostatics and demonstrate that a high-field site is responsible for the selectivity for small cations. Finally, we determine the energy barriers associated with the binding/unbinding of a Cl^- ion from the anion-binding site in the presence and absence of bound cations using umbrella sampling. Our results demonstrate that the affinity of different cations follows the apparent affinity observed in functional measurements on native kainate receptors and that anion binding is greatly facilitated by the presence of cations.

METHODS

General setup

Crystal structures for GluR5 complexes with the partial agonist kainic acid with Li^+, Na^+, and K^+ bound (Protein Data Bank (PDB) codes 3C31, 3C32, and 3C33, respectively) were used. Although the receptor is tetrameric in vivo and these crystal structures are dimers, there is a substantial amount of evidence (for a recent review see (2)) that suggests the extracellular ligand binding cores are arranged as a dimer of dimers and that the crystallographically observed dimers are functionally relevant. The crystal structures correspond to the residues 417–529 and 652–790 linked by a Gly-Thr linker and are thought to be an accurate reflection of the ligand-binding core in vivo (35). All MD simulations were performed using GROMACS Ver. 3.3.1 (36). The all-atom OPLS-AA force field (37,38) was used to describe ions and protein atoms. Production simulations were performed in an NPT ensemble maintained at 300 K and 1 bar pressure. The integration time step was set as 2 fs and a stochastic dynamics integrator (39) was used. The LINCS (40) algorithm was used to constrain protein bonds involving hydrogen atoms and SETTLE (41) for water molecules. Long-range electrostatics were treated using the particle mesh Ewald method (42) with a real-space cutoff of 10 Å. The van der Waals interactions were switched off smoothly between 8 and 9 Å, based on previous reports (43). Long-range dispersion correction was applied to energy and pressure to compensate for truncation effects. All crystal water molecules were retained and the protein was solvated in a cubic box of dimension $(90\ \text{Å})^3$ subjected to periodic boundary conditions. The TIP4P water model (44) was used for the initial MD simulations while the TIP3P water model (44) was chosen for the free energy calculations since, in our hands, this appeared to better reproduce the relative hydration free energy of ions (Table 1). Counterions were added to neutralize the simulation box and random water molecules were replaced with ions to make a 150-mM salt solution representing physiological conditions. Simulation data was analyzed using the GROMACS suite of tools and custom scripts, and visualized with VMD (45) and PyMOL (46). Images were generated with PyMOL.

The simulation protocol involved minimization of the system using the steepest descent algorithm with a force tolerance of 100 kJ mol^{-1} nm^{-1} (2.39 kcal mol^{-1} $Å^{-1}$). A 200-ps restrained run was then performed where the heavy atoms of the protein and ions were harmonically restrained using a force constant of 1000 kJ mol^{-1} nm^{-2} (2.39 kcal mol^{-1} $Å^{-2}$) to allow the solvent molecules to equilibrate around the protein. Production runs were performed after lifting these restraints. The data presented here equates to ~1.5 μs of all-atom simulations.

TABLE 1 ΔG_{water} (A→B) in TIP3P and TIP4P water models calculated using thermodynamic integration

Transformation	TIP3P	TIP4P	Experimental*
$Na^+ \rightarrow Li^+$	−24.20 ± 0.08	−27.70 ± 0.11	−26.30
$Li^+ \rightarrow Na^+$	24.23 ± 0.06	27.65 ± 0.18	26.30
$Na^+ \rightarrow K^+$	16.97 ± 0.02	19.92 ± 0.11	16.70
$K^+ \rightarrow Na^+$	−16.99 ± 0.02	−19.92 ± 0.10	−16.70
$Na^+ \rightarrow Rb^+$	21.86 ± 0.02	26.01 ± 0.13	21.50
$Rb^+ \rightarrow Na^+$	−21.83 ± 0.03	−26.13 ± 0.09	−21.50
$Na^+ \rightarrow Cs^+$	29.44 ± 0.06	35.66 ± 0.10	27.40
$Cs^+ \rightarrow Na^+$	29.44 ± 0.07	−35.75 ± 0.19	−27.40

*Marcus (50).

Thermodynamic integration and relative binding free energy

Table 2 summarizes the alchemical transformations performed in this study. GluR5 crystal structures solved with a range of ion species (34) were used for the forward and reverse calculations. Additional calculations were also performed on a structure of GluR6 complex with the full agonist glutamate to assess the influence of residues not conserved that were distant (>8 Å) from the binding site. Eleven equally spaced windows (λ = 0.0, 0.1 0.2, 0.3, 0.4, 0.5, 0.6, 0.7, 0.8, 0.9, 1.0) were used for each transformation. Simulations of 1 ns/λ were run for the ion transformations in water, whereas 6 ns/λ were used for the same transformation in the protein-ion complex. For each window, the structure was minimized and a short 200-ps run was performed with restraints imposed on ions and the heavy atoms of the protein. Free energy data $\partial U/\partial\lambda$, which is the derivative of the interaction energy, was written out every step. The first 1 ns of the production data was discarded as equilibration time. For block averaging, $\partial U/\partial\lambda$ was split into blocks of 500 ps after computing the statistical inefficiency (47). Using thermodynamic integration, the free energy change, ΔG, associated with transforming ion A ($\lambda = 0$) to ion B ($\lambda = 1$) is given by

$$\Delta G = \int_{\lambda=0}^{\lambda=1} \langle \partial U/\partial\lambda \rangle_{\lambda} d\lambda,$$

where $\langle \ldots \rangle$ represents an ensemble average. Numerical integration was performed using the trapezoidal rule. A thermodynamic cycle (Fig. 2) was used to calculate the relative binding free energy ($\Delta\Delta G$) of ions given by

$$\begin{aligned}\Delta\Delta G(\mathrm{A}\rightarrow\mathrm{B}) &= \Delta G_{\mathrm{bind}}(\mathrm{B}) - \Delta G_{\mathrm{bind}}(\mathrm{A}) \\ &= \Delta G_{\mathrm{protein}}(\mathrm{A}\rightarrow\mathrm{B}) - \Delta G_{\mathrm{water}}(\mathrm{A}\rightarrow\mathrm{B}).\end{aligned}$$

Here, $\Delta G_{\mathrm{protein}}(\mathrm{A}\rightarrow\mathrm{B})$ and $\Delta G_{\mathrm{water}}(\mathrm{A}\rightarrow\mathrm{B})$ are determined by alchemical transformation as described above.

TABLE 2 Structures used for calculating relative binding free energy ($\Delta G_{protein}$) using alchemical transformations

PDB ID	Resolution	Receptor	Details of structure	Transformation(s) performed
3C31	1.49 Å	GluR5	WT structure with bound Li^+	$Li^+ \rightarrow Na^+$
3C32	1.72 Å	GluR5	WT structure with bound Na^+	$Na^+ \rightarrow Li^+$
				$Na^+ \rightarrow K^+$
				$Na^+ \rightarrow Rb^+$
				$Na^+ \rightarrow Cs^+$
3C33	1.78 Å	GluR5	WT structure with bound K^+	$K^+ \rightarrow Na^+$
2I0B	1.96 Å	GluR6	Engineered structure with bound Na^+*	$Na^+ \rightarrow Li^+$
				$Na^+ \rightarrow K^+$
				$Na^+ \rightarrow Rb^+$
				$Na^+ \rightarrow Cs^+$

*The crystal structure is not wild-type. Therefore, in silico mutations (K494E, I749L, Q753K, E757Q) were made to make the wild-type sequence for the MD calculations.

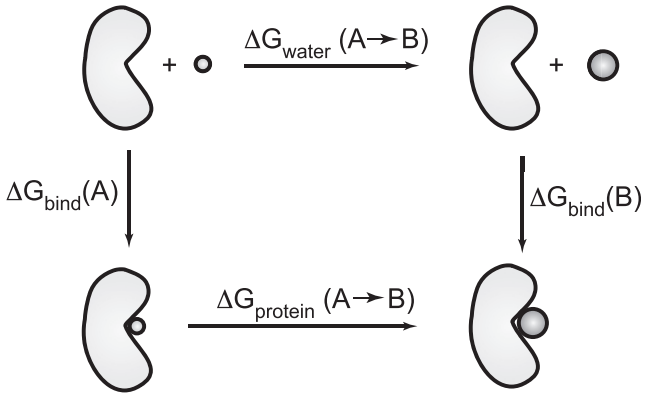

FIGURE 2 Thermodynamic cycle used to compute relative binding free energy. In this instance, A and B are cations. A is alchemically transformed to B, in bound and unbound states, and the ΔG of transformation calculated using thermodynamic integration. The relative binding free energy $\Delta\Delta G$ is calculated as $\Delta\Delta G(\mathrm{A}\rightarrow\mathrm{B}) = \Delta G_{\mathrm{bind}}(\mathrm{B}) - \Delta G_{\mathrm{bind}}(\mathrm{A}) = \Delta G_{\mathrm{protein}}(\mathrm{A}\rightarrow\mathrm{B}) - \Delta G_{\mathrm{water}}(\mathrm{A}\rightarrow\mathrm{B})$.

A reduced model of the binding site

To examine the mechanism of selectivity using a simple model, a reduced structure of the cation-binding environment was generated by extracting the residues and water molecules from the GluR5 Na^+-bound structure (PDB ID: 3C32) that lie within 10 Å of each cation. This included residues 487–491 (helix C), 504–516 (helix D/turn/strand 6), 751–768 (strand 13/turn/helix J), 39 water molecules, two Na^+ ions, and a Cl^- ion (Fig. 3 *A*). The extracted protein fragments were capped with acetyl and amide groups to mimic continuity. To preserve the structural integrity of the model, Cα atoms of all residues and oxygen atoms of all but two water molecules were harmonically restrained with a weak force constant 1000 kJ mol^{-1} nm^{-2} (2.4 kcal mol^{-1} $Å^{-2}$). The ions and two water molecules that coordinate the Na^+ ion were not restrained. Na^+ was alchemically transformed to K^+ in the binding site for a set of partial charges for the carboxylate group (Fig. 3 *B*) of Glu-509 and Asp-513 as shown in Table 3. Eleven intermediate λ-values (0.0, 0.1, 0.2, 0.3, 0.4, 0.5, 0.6, 0.7, 0.8, 0.9, and 1.0) were used with a simulation time of 1 ns/λ. Calculations were performed using a stochastic dynamics integrator at 300 K in vacuum with no periodic boundary conditions and all atoms were explicitly included in electrostatic calculations.

Potential of mean force of Cl^- unbinding

Since the two cation binding sites are related by the twofold axis of dimer symmetry with the buried anion site located on the dimer interface (Fig. 1), the reaction coordinate for Cl^- unbinding PMF calculations was chosen as the perpendicular bisector of the line segment joining the two cations that passed through the anion binding site (Fig. 4 *A*). This was taken as the *z* axis after aligning the protein structure. The GluR5 Na^+-bound

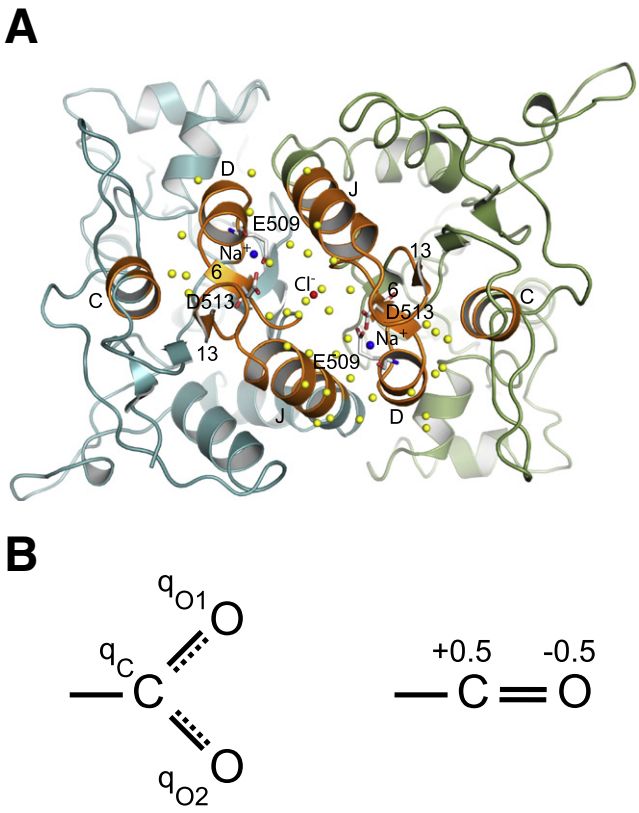

FIGURE 3 (*A*) Protein fragments used in the reduced model are shown in orange cartoon representation; the rest of the structure, which was omitted from the model, is colored as in Fig. 1 *A*. Refer to text and Table 3 for more details. Na^+ is shown as blue spheres, Cl^- as a red sphere, and water molecules as yellow spheres (spheres not to scale). Capital letters and numbers are used to indicate helices and strands, respectively. (*B*) Carboxylate and carbonyl groups with partial charges. Refer to Table 3 for carboxylate partial charges q_C, q_{O1}, and q_{O2} used in the reduced model.

structure (PDB ID: 3C32) was chosen for the PMF calculations. Twenty-five independent windows were used where the Cl^- ion was placed 0.5 Å apart, starting from the anion binding site and ending in bulk solution, taking it past three acidic residues (Glu-509, Asp-513, and Asp-761) and the highly mobile Arg-760 that acts as the lid of the anion binding site (15,34). For umbrella sampling, in each window, the Cl^- ion was harmonically constrained using a force constant of 5000 kJ mol^{-1} nm^{-2} (11.95 kcal mol^{-1} $Å^{-2}$). The reference was chosen as a set of Cα atoms from the D and J helices along with residues flanking this region (residues 505–515 and 747–774) that line the entry/exit pathway of the anion. Two sets of these simulations were performed, one in which the two cations were left in the cation binding sites and the other in which the cations were removed. To prevent the reaction pathway from being constantly moved by rotational and translational motion, the center-of-mass translation was removed and four Cα atoms, which were found to have low root mean-square fluctuation, were harmonically constrained. Production simulations consisted of 1.5 ns/window, the first 0.5 ns of which were discarded. Unbiased PMFs were obtained from the resulting umbrella sampling distributions with the weighted histogram analysis method (48) using code made available by Alan Grossfield (http://membrane.urmc.rochester.edu/wham/index.html).

TABLE 3 Relative binding free energy calculated using the reduced model (see text for more details) of the binding site

	Partial charges			
Run	q_C	q_{O1}	q_{O2}	$\Delta\Delta G$ ($Na^+ \rightarrow K^+$) (kcal/mol)
1*	0.7	−0.8	−0.8	6.63 ± 0.16
2	0.7	−0.7	−0.7	4.10 ± 0.13
3	0.6	−0.6	−0.6	2.29 ± 0.10
4	0.5	−0.5	−0.5	0.03 ± 0.09
5	0.4	−0.4	−0.4	−2.85 ± 0.07

Partial charges (Fig. 3 *B*) for carboxylate groups of Glu-509 and Asp-513 along with $\Delta\Delta G$ ($Na^+ \rightarrow K^+$) values for both cation binding sites combined are shown below.

*Asp and Glu carboxylate group partial charges from the OPLS-AA force field.

RESULTS

Selectivity of the binding site

Functional studies reveal that monovalent cations from the alkali metal family that modulate kainate receptors give different rates of desensitization (16,34). To elucidate the selectivity of the cation binding sites, we performed extensive relative binding free energy calculations using MD simulations of the GluR5 crystal structures with various cations bound as listed in Table 2. This involved transforming the ion, from say Na^+ to K^+, both in solution, and in the binding site, over 11 intermediate independent steps of 6 ns each. The obtained relative binding free energies are given in Table 4. This results in a rank order of binding of $Li^+ > Na^+ > K^+ > Rb^+ > Cs^+$, which is indicative of the selectivity of the binding site. Each cation is separated from the next member of the alkali metal family by ~3–5 kcal/mol, with a preference for smaller cations. For the start and end points, the forward and reverse transformations (Table 5) are in good agreement with other studies (49,50). The radial distribution functions also compare extremely well with experimental data (Table 6), suggesting the simulations are reasonably well converged. Although the crystal structures suggest that the cation is fivefold coordinated, during the course of all of these simulations and during those we previously reported (34), the side chain of Ile-755 moves away to allow a water molecule to form the sixth coordination site. Water molecules in these sites were observed to frequently swap with bulk water but analysis of 20-ns simulations clearly demonstrates that the spatial density optimizes the sixfold coordination of the sodium (see Supporting Material for more details).

Although the presence of bound cations affects the anion site, as discussed in the next section, the two cation sites appear to be independent. In a sequence of steps, we alchemically transformed Na^+ to K^+ in one site while keeping Na^+ in the second site. In a subsequent step, the second Na^+ was transformed to K^+. The sum of the free energy change in the two steps, which were both identical, resulted in a $\Delta\Delta G$ of 5.5 ± 0.1 kcal/mol, which is the same value obtained by transforming the two ions simultaneously (Table 4).

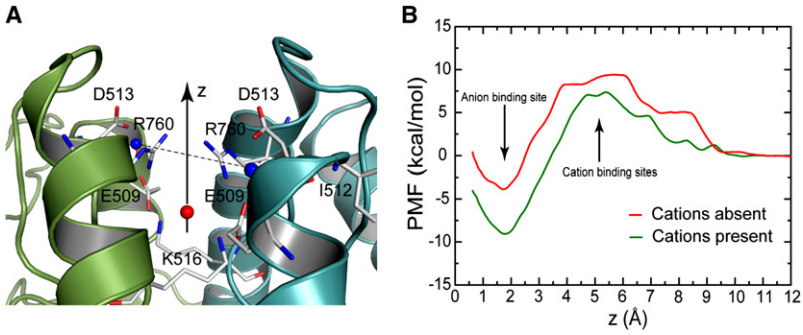

FIGURE 4 (*A*) Reaction coordinate used for computing the PMF for anion binding. The reaction coordinate was chosen as the perpendicular bisector of the line segment joining the centers of the two cation binding sites (*blue spheres*) and passing through the anion binding site (*red sphere*). (*B*) PMF profiles for the unbinding of the Cl^- ion in the presence (*green line*) and absence (*red line*) of bound cations. The location of the anion- and cation binding sites with respect to the chosen reference system are marked.

To assess how general this selectivity was within the family of kainate receptor subtypes and indeed to what extent, if at all, it is influenced by long-range interactions—due, for example, to differences in domain closure produced by full and partial agonists—we performed additional calculations on a wild-type (WT) model of the GluR6 receptor in complex with the full agonist glutamate (based on PDB code 2I0B, where four residues were mutated back to give the wild-type sequence. See Table 2). Both GluR5 and GluR6 are known to be allosterically modulated by cations and the cation binding site is conserved. The difference in RMSD between the two D1 domains (excluding loops 1 and 2) is 0.5 Å. Thus, this represents a test of how much the starting conformation and long-range effects from differences in sequence away from the binding site influence the free energy of binding. The results (Table 4) are identical to those obtained for GluR5. As the ion-binding pocket in kainate receptors is highly conserved, this suggests that the selectivity is controlled by local interactions and that long-range effects are relatively unimportant. To investigate to what extent the local interactions control the selectivity, we developed a simplified model of the binding sites (Fig. 3). Such a model has two advantages: 1), it is computationally cheaper; and 2), it allows us to explore key physical aspects that may contribute to the selectivity. Several studies on other proteins have arrived at the conclusion that a high charge field contributed by acidic residues would prefer Na^+ to K^+ (25,51). Initially, we started with the OPLS-AA force-field partial charges for the carboxylate group of Glu-509 and Asp-513 (Table 3, Run 1). Despite this simplification, the reduced model still produced a $\Delta\Delta G$ ($Na^+ \rightarrow K^+$) of 6.63 kcal/mol (Table 3), compared to the all-atom simulations that produced 5.5 kcal/mol (Table 4) for two binding sites. To study the effect of reducing the negative charge in the cation binding site, we systematically reduced the charge on the carboxylate groups as shown in Table 3). A reduction in the charge progressively makes the site less Na^+ selective and at run 4, which roughly represents a charge distribution similar to a carbonyl group (Fig. 3 *B*), the site is no longer Na^+-selective—suggesting that the high charge density is indeed the cause for Na^+ selectivity in this receptor. Functional experiments on the GluR6 E493Q mutant, which shows greatly reduced selectivity between monovalent cations, support this interpretation (34).

TABLE 4 Relative binding free energy ($\Delta\Delta G$) of cations in GluR5 structures. Errors are reported as the standard error of the difference of means

Transformation	GluR5 (kcal/mol)	GluR6* (kcal/mol)
$Na^+ \rightarrow Li^+$	−4.7 ± 0.1	−4.1 ± 0.1
$Li^+ \rightarrow Na^+$	4.7 ± 0.3	4.2 ± 0.1
$Na^+ \rightarrow K^+$	5.5 ± 0.2	5.2 ± 0.1
$K^+ \rightarrow Na^+$	−4.8 ± 0.2	−5.2 ± 0.1
$Na^+ \rightarrow Rb^+$	8.1 ± 0.2	7.7 ± 0.2
$Na^+ \rightarrow Cs^+$	11.6 ± 0.3	12.0 ± 0.4

*2I0B crystal structure is mutated back to WT (K494E, I749L, Q753K, E757Q) for MD simulations. Cations were modeled by replacing water molecules HOH119 and HOH180.

Cations modulate anion affinity

Two cations and an anion bind in the interfacial region between two subunits (Fig. 1) (15,34) and the apparent affinity for chloride increases with sodium concentration (34). To decipher the physical factors behind this, we first looked at the electrostatic field of the protein in the absence and presence of bound cations. As described previously, this clearly showed a reduction in the electronegative field above the surface of the anion binding site when cations were present (34) This suggests that the presence of bound cations could reduce the energy barrier and provide a more energetically favorable path for an anion to approach and bind in the

TABLE 5 The first maximum of the cation-oxygen radial distribution function from alchemical transformations with ions bound to GluR5

	$\lambda = 0$		$\lambda = 1$	
Transformation	Site 1 (Å)	Site 2 (Å)	Site 1 (Å)	Site 2 (Å)
$Na^+ \rightarrow Li^+$	2.3	2.4	2.0	2.0
$Li^+ \rightarrow Na^+$	2.0	2.0	2.3	2.4
$Na^+ \rightarrow K^+$	2.4	2.3	2.7	2.7
$K^+ \rightarrow Na^+$	2.7	2.6	2.4	2.4
$Na^+ \rightarrow Rb^+$	2.3	2.3	2.8	2.8
$Na^+ \rightarrow Cs^+$	2.3	2.3	3.0	3.0

For a transformation A → B, $\lambda = 0$ represents ion A and $\lambda = 1$ represents ion B. Ion-oxygen radial distribution function was computed over a 5-ns trajectory for each λ.

TABLE 6 The first maximum of the radial distribution function (RDF) of cation-oxygen atoms in the binding site from MD simulations of cation-bound structures

	First maximum (Å) of oxygen RDF from MD simulation		Average ion-oxygen distance (Å) from crystal structure		
Ion	Site 1	Site 2	Site 1	Site 2	Ion-oxygen distance (Å) (experimental (50))
Li^+	2.0	2.0	1.9*	1.9*	2.1
Na^+	2.4	2.4	2.3†	2.3†	2.4
K^+	2.7	2.8	2.8‡	2.8‡	2.8
Rb^+	2.8	2.8	2.9§	2.9§	2.9
Cs^+	3.0	3.0	3.0¶	3.1¶	3.1

As the position of the first maximum in the RDF describes the density of the oxygen atoms from the cation, we can compare this to the crystal structures.
*From crystal structure 3C31.
†From crystal structure 3C32.
‡From crystal structure 3C33.
§From crystal structure 3C34.
¶From crystal structure 3C35.

buried anion binding cavity. Hence, we constructed PMFs of Cl^- unbinding using umbrella sampling under two conditions: one where cations occupied the binding site, and the other where no cations were present in the binding site. Since the base of the anion binding site appears to be impermeable throughout the duration of all the simulations performed here, the preferred route of entry/exit would be through the top of the cavity with the flexible pair of Arg-760 acting as the lid (34). Therefore, we defined a reaction coordinate that is the perpendicular bisector of the line segment joining the two cation sites and passing through the anion binding site (Fig. 4 *A*). This is a reasonable assumption, given the fact that the buried site permits limited lateral motion, which would be well sampled in umbrella sampling simulations. The resulting unbiased PMF profiles of Cl^- unbinding in the presence and absence of cations are shown in Fig. 4 *B*. The profiles clearly show a reduction in the barrier, by ~2–5 kcal/mol along the path, encountered by the anion in the presence of cations. The barrier is introduced by three acidic residues, Glu-509, Asp-513, and Asp-761 that line the exit route of the anion. The presence of the cations makes anion binding a more favorable event by ~5 kcal/mol through the partial neutralization of the excess negative field introduced by the negatively-charged residues. This is also observable as a more favorable interaction energy for the anion in MD simulations and a more electronegative cavity from electrostatic surface potential analysis using the adaptive Poisson-Boltzmann solver (52) when cations are present.

DISCUSSION

Our approach allows the relative affinity for ion binding to kainate receptors to be calculated. This was not possible in prior experiments, which measured the effect of ions on the rate of desensitization triggered by application of glutamate (15,16), because the allosteric response triggered by agonists could not be separated from ion binding. Thus, in prior work the concentration response function for ion modulation measured both the affinity of ions for their binding sites, and the conformational change linking binding of glutamate to activation and subsequent desensitization of ion channel activity when both the anion and cation concentration was changed simultaneously. Here, we find that the binding affinity for cations follows the order $Li^+ > Na^+ > K^+ > Rb^+ > Cs^+$. The apparent affinity data from electrophysiological experiments, however, suggests that the order is $Na^+ > Li^+ > K^+ > Rb^+ > Cs^+$, with Na^+ being the most efficacious, but only by a small amount over Li^+ (34). A possible explanation is that the change in both anion and cation concentration lead to an underestimate of the apparent affinity for Li^+ in the functional experiments. It is also possible that although Li^+ binds more favorably, the complex interplay of events from binding to activation and desensitization would make Na^+ more efficacious, though the exact pathway still needs to be elucidated. Despite this, it is still quite remarkable that there is a correlation between the affinity calculated here and the apparent affinity derived from experiments that report a conformational change believed to be triggered by dimer dissociation rather than ion binding per se. Li^+ is often used for the treatment of mania in bipolar disorder (53) and replacing Na^+ with Li^+ in the extracellular region has been shown to potentiate GABA release from striatal neurons (54). The precise mode of action of Li^+-based treatments is currently unknown, but our results suggest that further work with kainate receptors, in this respect, would be intriguing.

To determine whether other proteins possess a similar Na^+ binding sequence motif as found in the kainate receptor (EKVID), we performed a BLAST (55) search of the Protein Data Bank. This produced over 100 homologous hits, but none had the same local conformation as observed in GluR5, nor did they appear to bind Na^+ ions, suggesting that, from currently known structures, the cation binding site sequence motif appears to be unique to the GluR family. Interestingly, thrombin, which is regulated by Na^+ binding (56), has a sequence motif QKVID. However, this segment has a totally different conformation from the EKVID observed for kainate receptors and the Na^+ binding site in thrombin identified from analysis of crystal structures (56) is located in another region of the protein. It is interesting to note the presence of a lysine in this motif in light of the DEKA motif in Na^+ channels, where it has been proposed to play an active role in selectivity (57). However, in this instance, the lysine does not interact either directly or indirectly with the binding-site residues and is unlikely to play a role in selectivity here.

The selectivity of the cation binding site in kainate receptors for smaller cations can be attributed to two factors, recently identified by Noskov and Roux (25) after an extensive survey of PDB structures with bound Na^+/K^+: 1),

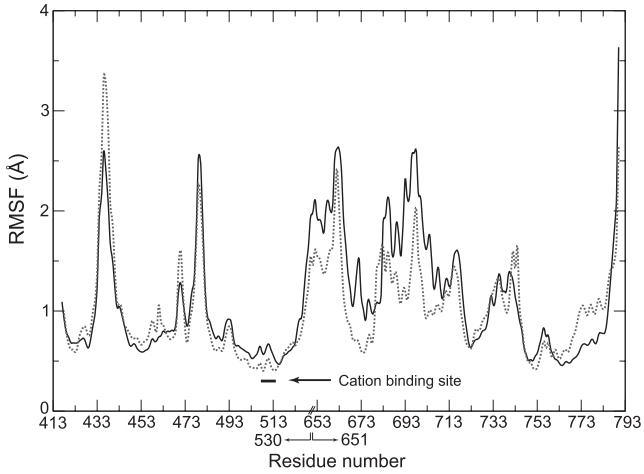

FIGURE 5 Root mean-square fluctuation (RMSF) of Cα atoms of the Na^+-bound GluR5 structure (PDB ID: 3C32) from a 20-ns MD simulation. The RMSF of the two subunits are shown in solid and dashed lines. Residues in the cation binding site (Glu-509, Ile-512, Asp-513) reside in a region, as marked, with low backbone movement.

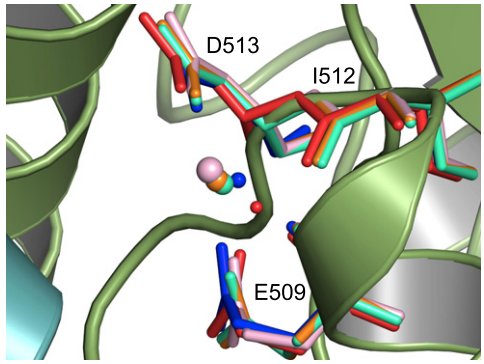

FIGURE 6 Cartoon representation of GluR5 crystal structures with binding site residues shown in stick representation and cations as spheres. Sphere radius corresponds to approximated ionic radius. Binding sites residues from the corresponding cation-bound crystal structures (3C31, 3C32, 3C33, 3C34, and 3C45) with cations shown as spheres; Li^+ (*red*), Na^+ (*blue*), K^+ (*green*), Rb^+ (*orange*), and Cs^+ (*pink*).

a region with highly charged electronegative ligands (49,58); and 2) the stiffness of binding site residues. Furthermore, their data showed that Na^+-binding sites frequently consisted of backbone and side-chain residues from residue 1, and its nearest neighbor $i\pm1$. In the kainate receptors, this motif is conserved and the ligand binding site consists of two acidic side chains GluR5–Glu-509 and Asp-513 along with backbone carbonyl groups of Glu-509 and Ile-512 resulting in a highly electronegative site, which is also apparent from the electrostatic calculations reported in Plested et al. (34). Additionally, analysis of the root mean-square fluctuation of the backbone Cα atoms of simulations (Fig. 5) showed that the residues involved in the binding site are indeed stiff and have some of the lowest fluctuations in the receptor (~0.5 Å). Additionally, charged residues like aspartate and glutamate on protein surfaces have been shown to prefer Na^+ over K^+ ions (51). The residues in the identified binding site are solvent-exposed and consist of two acidic side chains. Putting all of this together, it becomes apparent that the kainate receptor defines a site that has been tuned to select for a physiologically relevant small ion like Na^+. As the size of the cation increases, the ion is gently pushed out of the binding site to facilitate appropriate coordination of the ion owing to the rigid placement of carbonyl groups of Glu-509 and Ile-521 (Fig. 6). This pattern is also observed in the MD results as implied by the radial distribution function data (Table 6).

To test the hypothesis that the high charge field is a major cause of Na^+ selectivity in kainate receptors, we used a simplified model to manipulate the charge in the binding site. Such simplified toy models have been used in prior studies, e.g., to study the K^+ selectivity in potassium channels (59,60). However, an initial attempt to model the cation binding site using just carboxylate, carbonyl, and water atoms failed since the site is interconnected by a set of salt bridges, which keep the carboxylate groups in the appropriate orientation. A particularly crucial salt bridge is that between the side chain of E509 with the side chain of K516. K516 is also central to the formation of the anion binding site. A complete discussion of the salt-bridge network can be found in Plested et al. (34). Thus, a slightly enlarged system was tested with residues in the binding site free to move while the anion and its binding site residues were held fixed. These residues were included in the model to replicate the complex network of salt bridges, hydrogen bonds, and water bridges, which interconnects the two binding sites in the dimer crystal structures. Remarkably, this system is able to reproduce the relative binding free energy value of Na^+ versus K^+. Furthermore, a reduction in the negative field in the cavity makes it less favorable for Na^+, and as the charge on the carboxylate atoms was reduced (Table 3), the site becomes K^+ selective. At run 4, which represents a carbonyl-like charge distribution, but not geometry, the site is virtually nonselective. The stripped-down model can thus explain the origin of selectivity in this receptor and suggests a general principle for sodium selectivity along similar lines to that proposed by Noskov and Roux (25). Furthermore, variation of the strength of the harmonic restraint (with values of the force constant set at 250, 500, and 1000 kJ mol^{-1} nm^{-2} for either Cα atoms only or Cα and Cβ atoms) did not change the pattern of free energies with varying charge and only changed the absolute values by a maximum of 1.5 kcal/mol. With a force constant of 1000 kJ mol^{-1} nm^{-1} one would expect a fluctuation of ~0.2 Å. Weaker restraints will allow increased fluctuations. In the unconstrained full simulations, the root mean-square fluctuations (RMSFs) of the Cα atoms of the binding sites are ~0.5 Å (Fig. 5), suggesting that a restraint of 1000 kJ mol^{-1} nm^{-1} may be too stiff. However, the results appear to be robust to the exact choice of restraints imposed on the Cα atoms. This can be attributed to the

composition of the site where only two of the cation-coordinating groups are backbone carbonyls (and are thus heavily influenced by restraints imposed on the Cα atoms), but the remaining coordinating groups are relatively flexible acidic side chains or water molecules (Fig. 1 *C*). Although in this model we are effectively omitting long-range interactions, the difference in the free energy values calculated in the model system compared to the full structure suggests an effect of ~1 kcal/mol. Nevertheless, the model provides useful insight into the nature of cation selectivity in this system.

The cation and anion binding sites are located in the same dimer structure, are separated by ~8 Å (Fig. 1), and in functional studies show allosteric coupling. It was previously suggested that cations bind first, followed by the anion, and that they interact through a dipole mechanism (16). We believe, in the absence of any bound ions, the field around the anion binding site is too electronegative for efficient anion binding, due to a high energy barrier for anion approach. We proposed that cation binding reduces the field and provides a much more favorable environment for anion approach and binding. To test this, we performed umbrella sampling MD simulations on the GluR5 dimer to mimic the unbinding of Cl^- ion from its binding site, along a path that would take the anion into bulk solution via the opening of a lid residue that we previously identified as highly flexible (34). PMF profiles of Cl^- unbinding in the presence and absence of bound cations show that the presence of cations reduces the energy barrier by ~3 kcal/mol near the cation binding site. The anion binding site is also relatively more favorable by as much as 5 kcal/mol when Na^+ is bound. An accurate PMF is defined only when the ion is able to sample all possible confirmations. In the narrow cavity and entry/exit pathway, this is well defined due to very limited lateral movement. In this instance, we are interested in the relative difference in barriers in the absence and presence of cations by assuming that they are the same in bulk solution. Hence, differing from the mechanism proposed by Wong et al. (16), where for simplicity they assumed that the protein field is insignificant, we show that the protein field in the absence of cations provides a higher barrier for anions and the presence of cations diminishes the field, facilitating anion approach and binding. However, the PMF profiles suggest that even in the presence of cations there is still a large barrier of ~7 kcal/mol, which would prevent Cl^- binding to the resting or open state of the receptor. There are two things to consider here which bear on this interpretation. First, the pathway of Cl^- binding is a predetermined idealized trajectory, which might differ from the actual approach of an anion. (Although in this instance, the twofold symmetry of the interface suggests that this idealized pathway may be a reasonable first approximation.) Second, Cl^- binding may take place at a different conformational state of the receptor. Both of these factors could significantly reduce the barrier, but regardless, our results demonstrate that the Cl^- ion in the resting or active state of the receptor is stabilized substantially (5 kcal/mol) by the presence of the cation.

CONCLUSIONS

Using extensive MD simulations and free energy calculations, we have shown that the binding site selects for smaller cations and that the predictive selectivity agrees well with experimentally determined conclusions. Furthermore, the agreement between the free energy series from different kainate receptor subtypes suggests that the selectivity is controlled by local interactions. This result is also supported by the simplified model of the binding site, where the selectivity of a Na^+ ion over a K^+ ion could be attributed to the high electronegativity of the cation binding sites held on a rigid backbone. Furthermore, we demonstrate that the presence of cations stabilizes the anion by 5 kcal/mol and also appears to reduce the barrier along a simple unbinding trajectory. We also show that, even in the presence of cations, a large barrier still persists, suggesting that anion binding may either proceed in a different conformational state of the receptor, or that the whole process follows an alternative pathway. Structural information concerning the desensitized state will help to address this question.

SUPPORTING MATERIAL

One figure is available at http://www.biophysj.org/biophysj/supplemental/S0006-3495(09)00201-X.

We thank our colleagues Dr. Philip W. Fowler and Henry Chew for helpful discussions.

Computations were performed on the clusters of the UK National Grid Service and the Oxford Supercomputing Centre. P.C.B. is a Research Councils UK fellow. This work was supported by the Oxford University Clarendon Fund and UK Overseas Research Students Awards Scheme (to R.V.), Wellcome Trust (to P.C.B.), and the intramural research program of the National Institute of Child Health and Human Development, National Institutes of Health, Department of Health and Human Services (to M.L.M.).

REFERENCES

1. Dingledine, R., K. Borges, D. Bowie, and S. F. Traynelis. 1999. The glutamate receptor ion channels. *Pharmacol. Rev.* 51:7–61.
2. Mayer, M. L. 2006. Glutamate receptors at atomic resolution. *Nature.* 440:456–462.
3. Hollmann, M., and S. F. Heinemann. 1994. Cloned glutamate receptors. *Annu. Rev. Neurosci.* 17:31–108.
4. Yamakura, T., and K. Shimoji. 1999. Subunit and site specific pharmacology of the NMDA receptor channel. *Prog. Neurobiol.* 59:279–298.
5. Lerma, J., M. Morales, M. A. Vicente, and O. Herreras. 1997. Glutamate receptors of the kainate type and synaptic transmission. *Trends Neurosci.* 20:9–12.
6. Watkins, J. C., and D. E. Jane. 2006. The glutamate story. *Br. J. Pharmacol.* 147:S100–S108.
7. DeVries, S. H., and E. A. Schwartz. 1999. Kainate receptors mediate synaptic transmission between cones and "Off" bipolar cells in a mammalian retina. *Nature.* 397:157–160.

8. Kidd, F. L., and J. T. R. Isaac. 1999. Developmental and activity-dependent regulation of kainate receptors at thalamocortical synapses. *Nature*. 400:569–573.
9. Collins, K. D., G. W. Neilson, and J. E. Enderby. 2007. Ions in water: characterizing the forces that control chemical processes and biological structure. *Biophys. Chem.* 128:95–104.
10. Glossmann, H., and P. Presek. 1979. Alpha-noradrenergic receptors in brain membranes: sodium, magnesium and guanyl nucleotides modulate agonist binding. *Naunyn Schmiedebergs Arch. Pharmacol*. 306:67–73.
11. Mayer, M. L., L. Vyklicky, Jr., and G. L. Westbrook. 1989. Modulation of excitatory amino acid receptors by group IIB metal cations in cultured mouse hippocampal neurones. *J. Physiol*. 415:329–350.
12. Smart, T. G., X. Xie, and B. J. Krishek. 1994. Modulation of inhibitory and excitatory amino acid receptor ion channels by zinc. *Prog. Neurobiol*. 42:393–441.
13. Vernino, S., M. Amador, C. W. Luetje, J. Patrick, and J. A. Dani. 1992. Calcium modulation and high calcium permeability of neuronal nicotinic acetylcholine receptors. *Neuron*. 8:127–134.
14. Bowie, D. 2002. External anions and cations distinguish between AMPA and kainate receptor gating mechanisms. *J. Physiol*. 539:725–733.
15. Plested, A., and M. L. Mayer. 2007. Structure and mechanism of kainate receptor modulation by anions. *Neuron*. 53:829–841.
16. Wong, A. Y. C., D. M. MacLean, and D. Bowie. 2007. Na^+/Cl^- dipole couples agonist binding to kainate receptor activation. *J. Neurosci*. 27:6800–6809.
17. Arinaminpathy, Y., M. S. P. Sansom, and P. C. Biggin. 2002. Molecular dynamics simulations of the ligand binding domain of the ionotropic glutamate receptor $GluR^2$. *Biophys. J*. 82:676–683.
18. Arinaminpathy, Y., M. S. P. Sansom, and P. C. Biggin. 2006. Binding site flexibility: Molecular simulation of partial and full agonists within a glutamate receptor. *Mol. Pharm*. 69:11–18.
19. Kubo, M., and E. Ito. 2004. Structural dynamics of an ionotropic glutamate receptor. Proteins Struct. Funct. *Bioinf*. 56:411–419.
20. Lau, A. Y., and B. Roux. 2007. The free energy landscapes governing conformational changes in a glutamate receptor ligand binding domain. *Structure*. 15:1203–1214.
21. Mendieta, J., G. Ramirez, and F. Gago. 2001. Molecular dynamics simulations of the conformational changes of the glutamate receptor ligand binding core in the presence of glutamate and kainate. Proteins Struct. *Funct. Genet*. 44:460–469.
22. Speranskiy, K., and M. Kurnikova. 2005. On the binding determinants of the glutamate agonist with the glutamate receptor ligand binding domain. *Biochemistry*. 44:11508–11517.
23. Kollman, P. A. 1993. Free energy calculations: applications to chemical and biochemical phenomena. *Chem. Rev*. 93:2395–2417.
24. Mobley, D. L., J. D. Chodera, and K. A. Dill. 2006. On the use of orientational restraints and symmetry corrections in alchemical free energy calculations. *J. Chem. Phys*. 125:084902.
25. Noskov, S. Y., and B. Roux. 2008. Control of ion selectivity in LeuT: two Na_+ binding sites with two different mechanisms. *J. Mol. Biol*. 377:804–818.
26. Roux, B., M. Nina, R. Pomes, and J. C. Smith. 1996. Thermodynamic stability of water molecules in the bacteriorhodopsin proton channel: a molecular dynamics free energy perturbation study. *Biophys. J*. 71:670–681.
27. Roux, B. 1995. The calculation of the potential of mean force from computer simulations. *Comput. Phys. Commun*. 91:275–282.
28. Ivanov, I., X. Cheng, S. M. Sine, and J. A. McCammon. 2007. Barriers to ion translocation in cationic and anionic receptors from the *Cys*-loop family. *J. Am. Chem. Soc*. 129:8217–8224.
29. Khurana, E., S. O. Nielsen, B. Ensing, and M. L. Klein. 2006. Self-assembling cyclic peptides: molecular dynamics studies of dimers in polar and nonpolar solvents. *J. Phys. Chem. B*. 110:18965–18972.
30. Lu, D., P. Grayson, and K. Schulten. 2003. Glycerol conductance and physical asymmetry of the *Escherichia coli* glycerol facilitator GlpF. *Biophys. J*. 85:2977–2987.
31. Allen, T. W., O. S. Andersen, and B. Roux. 2004. Energetics of ion conduction through the gramicidin channel. *Proc. Natl. Acad. Sci. USA*. 101:117–122.
32. Beckstein, O., and M. S. P. Sansom. 2006. A hydrophobic gate in an ion channel: the closed state of the nicotinic acetylcholine receptor. *Phys. Biol*. 3:147–159.
33. Tieleman, D. P., and S. J. Marrink. 2006. Lipids out of equilibrium: energetics of desorption and pore mediated flip-flop. *J. Am. Chem. Soc*. 128:12462–12467.
34. Plested, A. J. R., R. Vijayan, P. C. Biggin, and M. L. Mayer. 2008. Molecular basis of kainate receptor modulation by sodium. *Neuron*. 58:720–735.
35. Deming, D., Q. Cheng, and V. Jayaraman. 2003. Is the isolated ligand binding domain a good model of the domain in the native receptor? J. Biol. Chem. 278:17589–17592.
36. van der Spoel, D., E. Lindahl, B. Hess, G. Groenhof, A. E. Mark, et al. 2005. GROMACS: fast, flexible and free. *J. Comput. Chem*. 26: 1701–1718.
37. Jorgensen, W. L., D. S. Maxwell, and J. Tirado-Rives. 1996. Development and testing of the OPLS all-atom force field on conformational energetics and properties of organic liquids. *J. Am. Chem. Soc*. 118:11225–11236.
38. Kaminski, G. A., R. A. Friesner, J. Tirado-Rives, and W. L. Jorgensen. 2001. Evaluation and reparameterization of the OPLS-AA force field for proteins via comparison with accurate quantum chemical calculations on peptides. *J. Phys. Chem. B*. 105:6474–6487.
39. Van Gunsteren, W. F., and H. J. C. Berendsen. 1988. A leap-frog algorithm for stochastic dynamics. *Mol. Simul*. 1:173–185.
40. Hess, B., J. Bekker, H. J. C. Berendsen, and J. G. E. M. Fraaije. 1997. LINCS: a linear constraint solver for molecular simulations. *J. Comput. Chem*. 18:1463–1472.
41. Miyamoto, S., and P. A. Kollman. 1992. SETTLE: an analytical version of the SHAKE and RATTLE algorithms for rigid water molecules. *J. Comput. Chem*. 18:1463–1472.
42. Essman, U., L. Perera, M. L. Berkowitz, T. Darden, H. Lee, et al. 1995. A smooth particle mesh Ewald method. *J. Chem. Phys*. 103:8577–8593.
43. Mobley, D. L., M. L. Dumont, J. D. Chodera, and K. A. Dill. 2007. Comparison of charge models for fixed-charged force fields: small molecule hydration free energies in explicit solvent. *J. Phys. Chem. B*. 111:2242–2254.
44. Jorgensen, W. L., J. Chandresekhar, J. D. Madura, R. W. Impey, and M. L. Klein. 1983. Comparison of simple potential functions for simulating liquid water. *J. Chem. Phys*. 79:926–935.
45. Humphrey, W., A. Dalke, and K. Schulten. 1996. VMD—visual molecular dynamics. *J. Mol. Graph*. 14:33–38.
46. DeLano, W. L. 2004. The PyMOL Molecular Graphics System. DeLano Scientific, San Carlos, CA.
47. Allen, M. P., and D. J. Tildesley. 1987. Computer Simulation of Liquids. Oxford University Press, Oxford.
48. Kumar, S., D. Bouzida, R. H. Swendsen, P. A. Kollman, and J. M. Rosenberg. 1992. The weighted histogram analysis method for free energy calculations of biomolecules. I. The method. *J. Comput. Chem*. 13:1011–1021.
49. Harding, M. 2002. Metal-ligand geometry relevant to proteins and in proteins: sodium and potassium. *Acta Crystallogr. D*. 58:872–874.
50. Marcus, Y. 1988. Ionic radii in aqueous solutions. *Chem. Rev*. 88:1475–1498.
51. Vrbka, L., J. Vondrasek, B. Jagoda-Cwiklik, R. Vacha, and P. Jungwirth. 2006. Quantification and rationalization of the higher affinity of sodium over potassium to protein surfaces. *Proc. Natl. Acad. Sci. USA*. 103:15440–15444.
52. Baker, N. A., D. Sept, S. Joseph, M. J. Holst, and J. A. McCammon. 2001. Electrostatics of nanosystems: application to microtubules and the ribosome. *Proc. Natl. Acad. Sci. USA*. 98:10037–10041.
53. Jope, R. S. 1999. Anti-bipolar therapy: mechanism of action of lithium. *Mol. Psychiatry*. 4:117–128.

54. Weiss, S., D. Kemp, L. Bauce, and F. Tse. 1990. Kainate receptors coupled to the evoked release of ^{3}H-γ-aminobutyric acid from striatal neurons in primary culture: potentiation by lithium ions. *Mol. Pharmacol.* 38:229–236.

55. Altschul, S. F., W. Gish, W. Miller, E. W. Myers, and D. J. Lipman. 1990. Basic local alignment search tool. *J. Mol. Biol.* 215:403–410.

56. Pineda, A. O., Z. -W. Chen, S. Caccia, A. M. Cantwell, S. N. Savvides, et al. 2004. The anticoagulant thrombin mutant W215A/E217A has a collapsed primary specificity pocket. *J. Biol. Chem.* 279: 39824–39828.

57. Tikhonov, D. B., and B. S. Zhorov. 2005. Modeling P-loops domain of sodium channel: homology with potassium channels and interaction with ligands. *Biophys. J.* 88:184–197.

58. Eisenman, G. 1962. Cation-selective glass electrodes and their mode of operation. *Biophys. J.* 2:259–323.

59. Noskov, S. Y., and B. Roux. 2006. Ion selectivity in potassium channels. *Biophys. Chem.* 124:279–291.

60. Noskov, S. Y., and B. Roux. 2007. Importance of hydration and dynamics on the selectivity of the KcsA and NaK channels. *J. Gen. Physiol.* 129:135–143.